

Interferometry following adaptive optics

Erez N. Ribak*

Department of Physics, Technion, Haifa 32000, Israel

ABSTRACT

Adaptive optics systems on single big telescopes correct many modes, allowing imaging in the infra red. At the same time, visible photons can be used as well, especially when infra red light is also employed for wave front sensing. It is argued that pupil-plane interferometry is the most useful application for high-resolution imaging. This is because the isoplanatic patch area and the integration time are larger after correction, and they afford enhanced signal collection in the aperture plane. In contrast, speckle imaging methods only gain indirectly from this enhancement.

Keywords: Stellar interferometry, adaptive optics, big telescopes, shearing interferometry.

1. THE IMPROVEMENT OF THE WAVE FRONT

Most big telescopes today measure the wave front and correct it using adaptive optics, and then use the corrected beam for infra-red observations. Since the correction in the infra red leaves the visible beam only partially corrected, the question arises: is there any use for the visible photons, and can something be gained from them? This is definitely important if the wave front sensing and the astronomical observation are performed in the infra red, essentially leaving all the visible photons unused. Similar questions occur in exoplanet search and in solar adaptive optics, where measurement and observation are performed with plentiful visible photons, but the quality of correction is not sufficient.

The best use for the visible light is for imaging, either directly or indirectly. There is a number of existing and new modes of observation, to be compared. Essentially, they are comprised of direct imaging and interferometric imaging. Spectral and coronagraphic information can be considered as the combination of the two. In the case of solar observations, the interferometric option is rather difficult, because of the large extent of the object.

First, what is to be expected from the partially corrected wave front? Let us assume that all aberrations, up to the highest corrigible by the adaptive optics system, are almost nulled. Since the fractal spectrum of aberrations is well described by the Kolomogorov-von Karman statistics, it can be drawn schematically in a log-log plot (Figure 1).

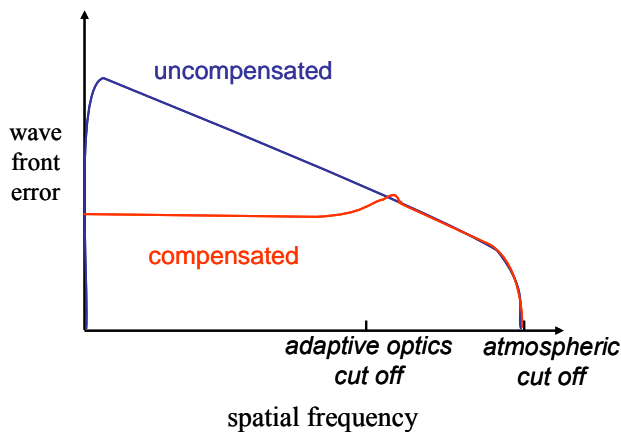


Figure 1: Wave front aberrations after partial correction are nearly constant all the way up to the adaptive optics pitch, then tails off following the Kolmogorov spectrum. This is a schematic log-log plot, and the small deviation near the adaptive optics cut off is due to aliasing effects and to non-circular optics, such as in the primary mirror or the deformable mirror.

* Visitor, Paris Observatory at Meudon, France. E-Mail eribak@physics.technion.ac.il

Thus the phase errors are reduced up to the pitch frequency of the elements of the deformable mirror, and for faint reference stars, by the pitch of the wave front sensor. A slight additional error might occur at higher frequencies because of aliasing in the adaptive optics system (e.g. the waffle mode or hexagonal mirrors). Alternative descriptions can be found in Roddier¹ and Cagigal and Canales². The region in which atmospheric aberrations are still not corrected is between r_0 and d_0 , the scales of Fried's parameter and the element size of the deformable mirror or wave front sensor. For different telescopes this range can lie between 5-40 cm and 30-100 cm (in the visible), according to the quality of the site, which also sets the decision of the size of d_0 .

As the spectrum of the residual aberrations can be considered flat up to the atmospheric cut off frequency, its effect on direct imaging will be to create a speckled background, which, upon integration, hides fine details. However, it is much improved compared to the uncompensated imaging case. This is because most of the coarse aberrations, those which cause most damage to the usual astronomical image, are essentially removed. For example, the tip-tilt error, which shifts the instantaneous stellar speckle pattern and causes it to smear upon integration, is rather small ($\approx \lambda / d_0$, from the simplified graph above).

Fried's coherence length, over which the standard deviation of the wave front does not exceed $\lambda / 2\pi \approx 80$ nm, will grow because of the partial correction of the wave front. Let us call it the compensated Fried's parameter, ρ_0 , where $\rho_0 \geq r_0$, with a similar effect in integration times². The Greenwood frequency, which is proportional to r_0 / w , where w is the wind speed¹. After correction, it is approximately proportional ρ_0 / w . Thus the isoplanatic volume, namely the product of the patch area and integration time, grows as $\rho_0^3 c / w$. The isoplanatic volume growth increases the number of coherent photons which can be detected (Figure 2). In pupil-plane interferometry and in aperture masking these parameters can set the maximum detector pixel size and the maximum integration time, and here is where there might be an advantage.

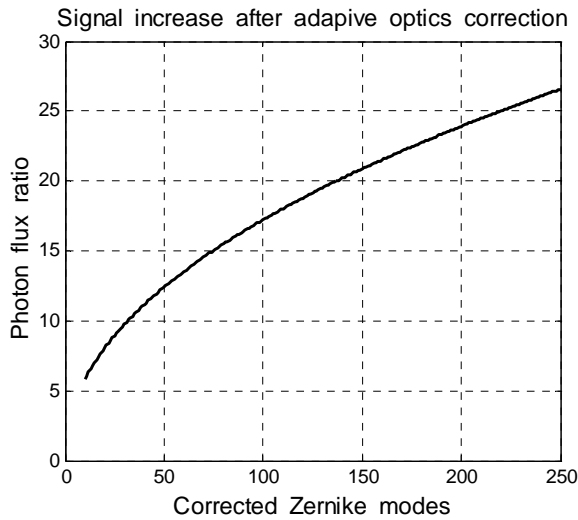


Figure 2 The size of the effective isoplanatic patch (over which the standard deviation of the wave front is less than one radian) grows with the quality of correction. For j ($j > 10$) corrected Zernike modes $\rho_0 \approx 1.25 j^{0.158} r_0$, independent of the telescope size. As a result, the photon flux inside an isoplanatic volume (patch area and duration) grows, as compared to the uncorrected case, by $1.95 j^{0.473}$.

2. SPECKLE IMAGING AND INTERFEROMETRY

Thus there are two modes of direct imaging which can be considered: by integration and by speckle imaging. Direct imaging might suffer from smearing of fine details and high background, but the images will be rather stable. When speckle imaging is performed, it is also simpler than uncompensated speckle imaging. Again, because of the very small shift of the central speckle, shift-and-add methods will require less of the shift, more of the smart add. Such methods act in a manner of blind deconvolution³. This deconvolution can also be accomplished by fitting the wave front, measured separately⁴, or from its instantaneous power spectrum, calculated from matched filtering of the speckles⁵. Similar methods integrate over the Fourier transform or the wave front⁶ or closure phase in triple correlation⁷. The dark speckle method for search for faint stellar companions seems to be the first application of post-correction interferometry⁸.

These speckle imaging methods will be easier to perform following the partial correction, but will also require a fast speckle camera (although the speckle rate will be slower now). For the wave front deconvolution method they will require also a separate wave front sensor, one that is tuned to the residual – and reduced – error spectrum. Also the rate of measurements will be lower due to the reduction of aberrations. The pixel scale in the imaging camera will still be needed to be diffraction-size limited, but some of the processing can be over coarser image or Fourier coordinates and hence more robust to noise. Some of these attributes are being used in solar adaptive optics for improved resolution in the visible⁹.

Regarding interferometric imaging, there are a number of well-developed and new methods which can be applied. They tend to measure the interference in the pupil plane, where the gain in integration volume is direct^{10,11}. Folding, lateral, and rotational shear interferometers (Figure 3) are well established^{12,13,14,15,16,17}. Lateral shear interferometers are redundant (all fringes belong with the same base-line) and thus their pixel size is limited only by ρ_0 . However, because of this redundancy they do not allow phase integration or phase closure. In addition, they have to be scanned in r - θ space. They have an advantage in that they are also inherently white light interferometers, and do not need any colour correction.

Folding shear interferometers and rotational shear interferometers are not redundant, and hence their pixel size can be limited by spatial accuracy in the u - v domain, and not by ρ_0 . This means that if the pixels are too large, they might average over many spatial frequencies. Folding shear interferometers require additionally scanning in θ space.

In contrast with these, rotational shear interferometers allow either phase closure (at 120° shear) or Knox-Thompson processing (at $180^\circ - \rho_0 / R$) as will be explained below^{18,19}. Since the interferogram is missing its central part, hidden by the central obscuration of the telescope, there is a need to take another measurement off centre.

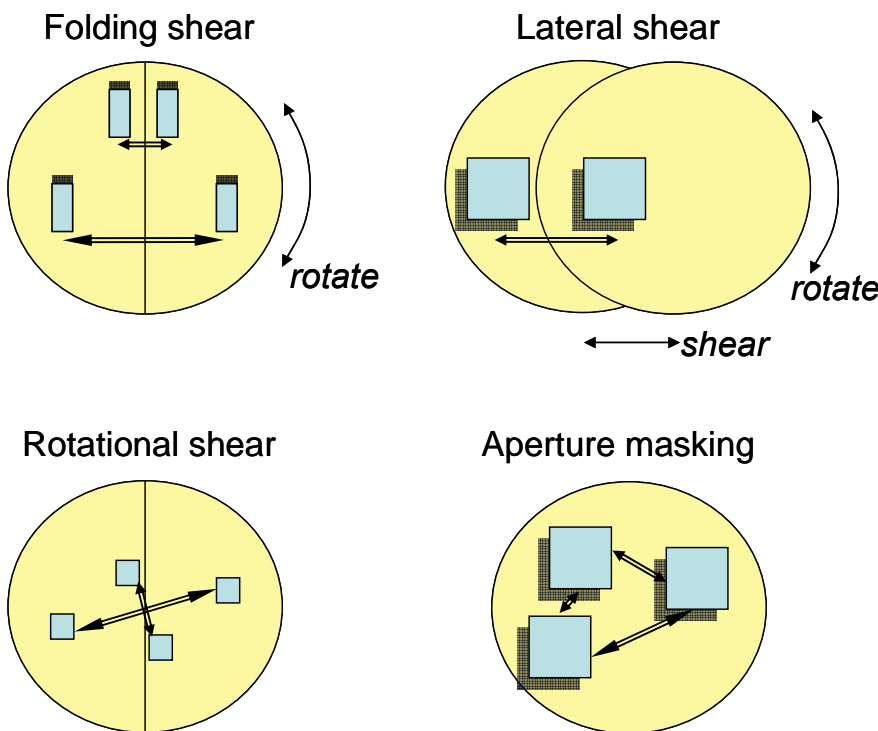


Figure 3: It is possible to extend the aperture or pixel size up to the corrected correlation length ρ_0 in the directions marked by a shadow. In the other direction it might be limited by u - v blurring. In the case of lateral (and constant) shear, both extension directions are possible. In folding shear, extension and shear are orthogonal directions. In aperture masking, between any two apertures the extension is normal to the connecting u - v vector. The central obscuration is not shown, and its lack in rotational shear means the loss of low frequencies.

In aperture masking there will be now a similar requirement, where the mask hole size will also be set by ρ_0 and be the requirement not to have spatial mixing. Either directly imaging in the focal plane, or using a set of lenslet-fed fibres to achieve multiple interference between the fibres^{20,21}, the hole size or the lenslet size will be set by these two parameters.

3. PHASE INFORMATION

Phase integration and phase closure play a significant role, where they are possible. Phase closure can be obtained in the simplest case by having a rotational shear of $2\pi / (2n+1)$ for any positive integer n ¹⁸. For example, in the case of $2\pi / 3$ shear, an interferogram pixel corresponds to two aperture areas separated by a vector u_1 of angular extent of $2\pi / 3$. Another pixel of $2\pi / 3$ rotation corresponds to two aperture areas, one overlapping a previous one, and the other of $2\pi / 3$ away. A third pixel on this equilateral triangle will correspond to two areas overlapping one each of the previous two, forming closure in the aperture (Figure 4).

Phase integration through Knox-Thompson averaging is possible by using a rotational shear of $2\pi / n - \rho_0 / 2R$ for any integer $n > 1$ ¹⁸. Thus every pixel in the interferogram corresponds to almost two opposite areas in the telescope aperture. The opposite *interferogram* pixel, across the diameter line, corresponds to two opposite areas in the aperture, one of which overlaps one of the previous areas, while the other partly overlaps it. Hence the interferogram is measured at two vectors whose difference in the aperture is $\rho_0 / 2$. Averaging is performed over many atmospheric realizations. Otherwise, it is possible to achieve similar results using non-overlapping paths^{19,22} or a combination of the two methods.

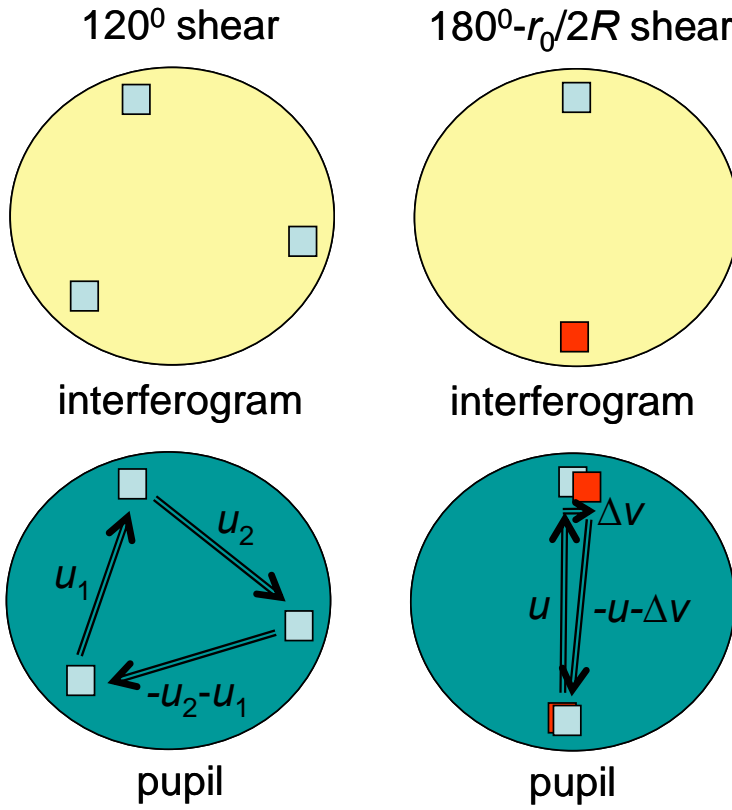


Figure 4: Left: phase closure in $2\pi/3$ shear: every three points in an equilateral triangle in the interferogram (top) correspond to an equilateral closure triangle in the telescope aperture (bottom). Right: Knox-Thompson integration in the pupil is achieved by two opposite pixels in an interferogram which is between two images of the aperture, one rotated by π plus an additional maximal rotation of $\rho_0/2$ at the perimeter. The top interferogram pixel corresponds to two points in the aperture, and the bottom pixel corresponds to two points, one of which differs by $\rho_0/2$ from the previous one. Integration around the centre yields the tangential component. In the 180° rotation the maximum spatial frequency is larger by $\sqrt{3}/2$ than that at 120° . The central obscuration is not shown.

The importance of colour correction is high, especially for the low signal case, where one wishes to integrate over many wave lengths simultaneously. While speckle imaging and lateral shear interferometry need no such correction, all others methods do. It is not clear how narrow the corrected speckle field is, but for very narrow speckle imaging, such as dark speckle⁸, colour correction is useful. This is because the fringe density varies with the wave length, and fringes of different colours mix on the detector. Only the central, white light fringes (as set by the spectral width detected) are useful. If one uses a chromatising device, which magnifies the sources according to their colours, the resulting fringes at different colours will have the same spacing and will have a much higher contrast (or wider extent). This was achieved in the past^{23,24,8}. A similar device is proposed now for fibre beam combination in speckle masking, when it is not following the Fizeau or Michelson schemes²⁵.

The complexity of the observed object is also important. While speckle methods are hardly influenced by extended objects, interferometric imaging suffers from reduction in the signal-to-noise ratio as the object becomes more complex²⁶. In general, interferometers are preferred to simple speckle methods¹⁹, but the assumptions in that study were that speckle methods were limited to signal-to-noise ratio of unity, and that one observes point sources. Both of these assumptions do not hold in most cases. Thus, one should decide according to the complexity of the object which method to use. Notice that the complexity of the object is not necessarily its extent. This is because in many cases there are prior assumptions about the object, such as in search for planets next to a star, in binary measurements, in stellar discs and more. A simple model can be fitted to the observed data with quite a few parameters, independent of the size of the object.

Thus, there is a number of options for interferometric imaging, each with its advantages and drawbacks. For the comparison, it is assumed that all use a fast photon camera and avoid additional wave front sensing in the visible. Estimates are summarized in the table.

	Speckle Imaging	Interferometry					
Processing Method	Blind deconvolution, Triple correlation ,,,	Aperture masking	Aperture fibres	Lateral shear	Folding shear	Rotational shear $2\pi/3$	Rotational shear $\pi-\rho_0/D$
$u-v$ coverage Solution	Full	Partial Scan $u-v$	Partial Scan $u-v$	Single Scan $r-\theta$	Line Scan θ	Small Ring Decentre	Max Ring Decentre
Gain from $\rho_0 > r_0$	Some During processing	Large	Large	Largest	Large	Large	Large
$\Delta\lambda$ λ correction	Narrow No	Narrow Wide	Narrow Wide	Wide	Narrow Wide	Narrow Wide	Narrow Wide
Phase closure	Calculated	Measured	Measured	No	No	Measured	Calculated
Object extent complexity	Large Complex	Small Simple	Small Simple	Small Simple	Small Simple	Small Simple	Small Simple

4. ACKNOWLEDGEMENTS

I wish to thank Pierre Lena and the interferometry group at Meudon for their kind hospitality. Comments by Guy Perrin helped improve this work.

5. REFERENCES

1. F. Roddier (1999), *Adaptive optics in astronomy*, Cambridge University Press.
2. M. P. Cagigal and V. F. Canales, Generalized Fried parameter after adaptive optics partial wave-front compensation, *J. Opt. Soc. Am. A*, **17**, 903-10 (2000), Residual phase variance in partial correction: application to the estimate of the light intensity statistics, *ibid*, 1312-8. V. F. Canales and M. P. Cagigal, Gain estimate for exoplanet detection with adaptive optics, *Astron. Astroph. Suppl. Series* **145**, 445-9 (2000).
3. G. R. Ayers and J. C. Dainty, Iterative blind deconvolution and its applications, *Opt. Lett.* **13**, 547-9 (1988).
4. J. Primot, G. Rousset, and J. C. Fontanella, Deconvolution from wave front sensing: a new technique for compensating turbulence-degraded images, *J. Opt. Soc. Am. A*, **7**, 1589-608 (1990).
5. E. Ribak, Astronomical imaging by filtered, weighted shift-and-add technique. *J. Opt. Soc. Am.* **A 3**, 2069-77 (1986).
6. K. T. Knox and B. J. Thompson, Recovery of images from atmospherically degraded short-exposure photographs, *Astrophys.J.* **193**, L45-8 (1974).
7. A. Lohmann, W. G. Weigelt, and B. Wirtzner, Speckle masking in astronomy: triple correlation theory and applications, *Appl. Opt.* **22**, 4028-37 (1983).
8. A. Boccaletti, C. Moutou, A. Labeyrie, D. Kohler, and F. Vakili, Present performance of the dark-speckle coronagraph, *Astron. Astrophys. Suppl. Ser.* **133**, 395-402 (1998).
9. C. Denker, D. Mascarinas, Y. Xu, W. Cao, G. Yang, H. Wang, P. R. Goode and T. Rimmele, High-spatial resolution combining high-order adaptive optics, frame selection, and speckle masking reconstruction, Submitted to *Solar Physics* (2004). <http://solar.njit.edu/preprints/denker1223.pdf>
10. F. Roddier, Interferometric imaging in optical astronomy, *Phys. Rep.* **170**, 97-166 (1988).
11. K. Itoh and Y. Ohtsuka, Fourier-transform spectral imaging: retrieval of source information from three-dimensional spatial coherence, *J. Opt. Soc. Am. A* **3**, 94-100 (1986). K. Itoh, T. Inoue, and Y. Ichioka, Interferometric spectral imaging and optical three-dimensional Fourier transformation, *J. Appl. Phys* **29**, L1561-4 (1990).
12. J. D. Armitage and A. Lohmann, Rotary shearing interferometry, *Opt. Acta* **12**, 185-92 (1965).
13. J. B. Breckinridge, Coherence Interferometer and Astronomical Applications. *Appl. Opt.* **11**, 2996-3003 (1972).
14. J C Dainty and R J Scaddan, A coherence interferometer for direct measurement of the atmospheric transfer function, *Mon. Not. R. Astr. Soc.* **167**, 690-730 (1974).
15. C. Roddier and F. Roddier, High angular resolution observations of alpha Orionis with a rotation shear interferometer. *Astroph. J.* **270** L23-6 (1983).
16. E. Ribak and E. Leibowitz, Shearing Stellar interferometer: 1. Digital data analysis scheme. *Appl. Opt.* **24**, 3088-93 (1985). E. Ribak, E. Leibowitz, and E. K. Hege, Shearing Stellar interferometer: 2. Opto-electronic phase-locked system. *ibid*, 3094-108.
17. J.-M. Mariotti, J.-L. Monin, P. Ghez, C. Perrier, A. Zdrozny, Pupil plane interferometry in the near infrared. I - Methodology of observation and first results, *Astron. Astroph.* **255**, 462 (1992).
18. E. Ribak, Phase closure with a rotational shear interferometer. *Appl. Opt.* **26**, 196-8; (1988). Phase relations and imaging in pupil plane interferometry. *NOAO-ESO Conference on High Resolution Imaging by Interferometry*, Munich (1987).
19. A. Chelli and J. M. Mariotti, Visibility and phase analysis for image and pupil plane interferometry at optical wavelengths, *Astron. Astroph.* **157**, 372-82 (1986).
20. S. Lacour, G. Perrin, J. Woillez, F. Assemat, T. Eric, Aperture masking interferometry and single-mode fibers, *SPIE* **5491**-153, W. A. Traub, ed. (2004).
21. E. Tatulli, P. Mege, A. Chelli (2004), Single-Mode versus multimode interferometry: a performance study, *Astron. Astroph.* **418**, 1179-86.
22. J.-L. Monin, J.-M. Mariotti, P. Ghez, C. Perrier, L. Desbat, Pupil plane interferometry in the near infrared. II - Phase recovery and image reconstructions *Astron. Astroph.* **260**, 510 (1992).
23. C. Roddier, F. Roddier, F. Martin, A. Baranne, R. Brun, Twin-image holography with spectrally broad light. *J. Optics* **11**, 149-52 (1980).
24. C. G. Wynne (1979), Extending the bandwidth of speckle interferometry. *Opt. Comm.* **28**, 21-5.
25. E. N. Ribak, G. Perrin, and S. Lacour, Multiple beam combination for faint objects, *SPIE* **5491**-216, W. A. Traub, ed. (2004).
26. E. Ribak, F. Roddier, C. Roddier and J. B. Breckinridge, Signal to noise ratio in white light holography, *Appl. Opt.* **27**, 1183-8 (1988).